Solid-State NMR Investigation of the Buried X−Proline Peptide Bonds of Bacteriorhodopsin†

Jonathan C. Lansing,‡,⊥ Jingui G. Hu,‡,§,|| Marina Belenky,|| Robert G. Griffin,‡ and Judith Herzfeld*,||

Department of Chemistry and Center for Magnetic Resonance, Francis Bitter Magnet Laboratory, Massachusetts Institute of Technology, Cambridge, Massachusetts 02139-4307, and Department of Chemistry and Keck Institute for Cellular Visualization, Brandeis University, Waltham, Massachusetts 02454-9110

Received October 21, 2002; Revised Manuscript Received January 27, 2003

ABSTRACT: The role of proline residues in the photocycle of bacteriorhodopsin (bR) is addressed using solid-state NMR. ^{13}C and ^{15}N chemical shifts from X−Pro peptide bonds in bR are assigned from REDOR difference spectra of pairwise labeled samples, and correlations of chemical shifts with structure are explored in a series of X−Pro model compounds. Results for the three membrane-embedded X−Pro bonds of bR indicate only slight changes in the transition from the resting state of the protein to either the early or late M state of the protonmotive photocycle. These results suggest that the buried prolines serve a principally structural role in bR.

Bacteriorhodopsin (bR)[1] is a heptahelical integral membrane protein with an embedded retinylidene chromophore. In a multistep photocycle, the light absorbed by the chromophore drives proton transport across the cell membrane. The key to this vectorial action is the release of the chromophore proton to the extracellular half-channel and the subsequent replacement of the chromophore proton from the intracellular half-channel. Protein structural rearrangements also occur during this pump cycle. However, the details of these structural changes remain unclear, as does their relevance to the critical switch in the connectivity of the Schiff base between the two sides of the membrane while it is deprotonated (i.e., during the lifetime of the M intermediate).

Special opportunities for structural change are presented by the proline residues in bR. Proline is the only naturally occurring secondary amino acid, with its side chain looping back to form a covalent linkage to the nitrogen. Two special properties result from this unique structure. First, the proline nitrogen cannot participate in typical hydrogen-bonding interactions as it cannot serve as a hydrogen bond donor. Second, the *cis* conformation of the X−Pro peptide bond is accessible due to steric destabilization of the *trans* conformation (Figure 1). The implications of these unique properties are both structural and dynamical. Structurally, proline is typically found to act as a helix breaker, with proline-induced kinks ranging from 15° to 40° (*1*, *2*). As such, it is surprising that of the 11 proline residues in bR, three, Pro50, Pro91, and Pro186, are located in helices B, C, and F, respectively. X−Pro bonds have also been suggested to serve key dynamic roles in proteins generally (*3*, *4*) and in bacteriorhodopsin in particular (*5*, *6*). In bR, the buried proline residues have received considerable attention, centered on the question of whether they serve a structural or a dynamic role (*5*−*9*).

Mutagenesis indicates that none of the buried prolines is irreplaceable, yet mutation of any of these three prolines significantly alters protein function. As the proline nitrogen cannot act as a hydrogen bond donor, it leaves a free carboxyl group in the $i - 4$ position that can hydrogen bond to other parts of the protein. Mutation of Pro50 or Pro91 to either Ala or Gly removes these interhelical hydrogen bonds and slows the folding of the apoprotein (*9*). Mutation of any of the buried prolines results in altered regeneration of the apoprotein with retinal (*9*, *10*), suggesting that the proline residues are important for the formation of the retinylidene binding pocket. The influence of the buried prolines on the chromophore environment has been demonstrated by altered chromophore HOOP modes resulting from P50A, P91A, P91G, P186A, and P186G mutations (*11*). In Pro186 mutants, the C−C and C═C stretch modes of the chromophore are altered as well (*11*). Schiff base deprotonation and reprotonation rates are also altered by mutations of any buried proline residue (*12*), and pump activity is dramatically decreased, especially for mutations of Pro186 (*10*).

† This research was supported by NIH Grants GM-36810, GM-23289, and RR-00995.

* To whom correspondence should be addressed. E-mail: herzfeld@brandeis.edu. Telephone: 781-736-2538. Fax: 781-736-2516.

‡ Massachusetts Institute of Technology.

⊥ Present address: Department of Molecular Biology and The Skaggs Institute for Chemical Biology, The Scripps Research Institute, La Jolla, CA 92037.

§ Present address: Materials Research Laboratory, University of California Santa Barbara, Santa Barbara, CA 93106.

|| Brandeis University.

[1] Abbreviations: bR, bacteriorhodopsin; NMR, nuclear magnetic resonance; FTIR, Fourier transform infrared; rf, radio frequency; WT, wild type; PM, purple membrane; CP, cross polarization; CW, continuous wave; TPPM, two pulse phase modulation; REDOR, rotational-echo double resonance; DA, the dark-adapted form of bR which consists of a mixture of bR_{568} and bR_{555}; LA, the light-adapted form of bR which is composed solely of bR_{568} and serves as the photon receptor for the protonmotive photocycle; M_o and M_n, photocycle intermediates with a deprotonated Schiff base, the latter a thermal relaxation product of the former; M_N, the intermediate in the D96N mutant with a deprotonated Schiff base and an N-like protein conformation; N, the intermediate occurring immediately after reprotonation of the Schiff base.

10.1021/bi027042f CCC: $25.00
Published on Web 03/05/2003

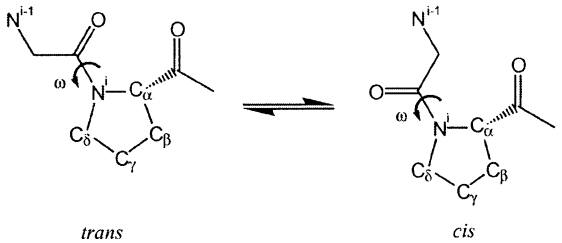

FIGURE 1: The *cis*−*trans* isomerization of the X−Pro peptide bond.

Time-resolved FTIR spectroscopy of isotopically labeled bR has been used to probe the role of proline residues throughout the photocycle. By comparing the vibrational spectra of various intermediates, changes in the vibration frequencies can be identified. Using this approach, two groups have demonstrated that at least one X−Pro bond has a perturbed C−N stretch in the K state which persists in the M state (*6*, *13*) and that the Tyr185−Pro186 bond has a perturbed C═O stretch in the N photocycle intermediate (*14*). Pro186 mutants also reduced the intensity of amide I and II difference bands in M, indicating that secondary structural changes during the photocycle are facilitated by the presence of Pro186 (*11*). In addition, mutation of Pro186 eliminated the perturbations of the C═O stretch bands associated with Asp96 that are normally seen in the bR → M transition (*11*).

Large-scale structural rearrangements of bR have been observed by cryoelectron microscopy of photocycle intermediates. In wild-type (WT) bR in its native 2D crystal lattice, motions of the F and G helices occur during the lifetime of M and persist through the latter part of the photocycle (*15*, *16*). These motions have the effect of widening the cytoplasmic end of the transport channel. While Pro186 would seem a likely candidate for the hinge point of helix F, high-resolution X-ray crystal structures of the late M state have not demonstrated a pivotal role for proline. The structure obtained for the M_N intermediate of D96N shows disordering of helix F that originates near Asn176, although no consistent tilt is observed (*17*). The crystal structure for the M intermediate of the WT protein indicates tilting of the F helix, with the bend distributed from Leu174 to Asn176 (*18*). However, neither X-ray structure exhibits motions of the same magnitude or direction as indicated by the cryoelectron microscopy of native membranes (*16*). This raises the question of whether crystal packing forces may be altering the photocycle in the 3D crystals. Conformational selection by crystal packing forces is not unprecedented; the crystal structure of the cyclophilin A complex with the HIV-1 capsid protein indicates a single conformation about the Pro90 peptide bond (*19*), while NMR exchange spectroscopy demonstrates the *cis/trans* isomerization of the Pro90 bond in vitro (*20*).

To date, NMR investigations of the proline peptide bond configurations in bR have been limited to the resting state. Spectra of monomeric [γ-^{13}C]Pro-bR were obtained in the solvent mixture $CHCl_3$:CD_3OD + 0.1 M $LiClO_4$ (*5*). From the $^{13}C\gamma$ chemical shifts, which are diagnostic for the X−Pro conformation, it was concluded that all of the X−Pro bonds in this preparation are *trans*. However, the color change from the normal purple to a brownish yellow in this solvent suggests the possibility of a non-native structure for the solubilized bR. More definitive results were established by solid-state NMR studies of [β-^{13}C]Pro-bR and [γ-^{13}C]Pro-bR in the native purple membrane (PM) (*8*). The chemical shift difference between the β and γ carbons indicates that all of the prolines in native light-adapted (LA) bR are in the *trans* conformation. The *trans* conformation of the X−Pro peptide bonds in the LA state was subsequently confirmed by X-ray crystallography (*21*−*23*).

Here we present solid-state NMR investigations of the three buried X−Pro peptide bonds in three different states of bR. ^{13}C and ^{15}N chemical shift tensors are determined in model X−Pro peptides to investigate correlations between chemical shifts and structural parameters. The isotropic ^{13}C and ^{15}N chemical shifts of the buried X−Pro bonds of bR, which are selected by amino acid sequence, are measured in the LA, M_o, and M_n intermediates of the photocycle. We find that the chemical shifts are only slightly perturbed in both the early and late M states, suggesting that little structural change occurs at these X−Pro peptide bonds.

MATERIALS AND METHODS

Model Peptides. Ala-Pro-Gly, Boc-Ala-Pro, cyclo-(Pro-Leu), cyclo-(Pro-Pro), and Z-Pro-Pro were purchased from Bachem Bioscience Inc. Pr-Pro and cyclo-(Pro-Met) were synthesized as described below. The remaining peptides were purchased from Sigma Chemical Co.

Synthesis of Pr-Pro. The synthesis of Pr-Pro was based on the protocol for synthesis of carbobenzoxyglycine (*24*). A solution of 100 mmol of proline in 25 mL of 4 N NaOH was chilled to ca. 0 °C. A total of 30 mL of 4 N NaOH and 110 mmol of propionyl chloride were added alternately in five aliquots over the course of 20−30 min with vigorous shaking and cooling in an ice bath. The reaction mixture was kept alkaline at all times by the addition of NaOH as required. Upon completion of the reaction, the excess acid chloride was extracted with 20 mL of ether. The aqueous fraction was acidified slowly to Congo red with 5 N HCl while being cooled in an ice bath. After 30 min of cooling, the crystalline propionylproline was filtered and dried before recrystallization from ethyl acetate.

Synthesis of Cyclo-(*Met-Pro*). The cyclic peptide was prepared according to the protocol of Padmanabhan and Jakkal (*25*). The linear Met-Pro peptide was dissolved in water and the solvent allowed to evaporate slowly, producing colorless crystals of the cyclic peptide.

bR Sample Preparation. [1-^{13}C]Thr-[^{15}N]Pro-[ζ-^{15}N]Lys-bR, [1-^{13}C]Tyr-[^{15}N]Pro-[ζ-^{15}N]Lys-bR, and [1-^{13}C]Val-[^{15}N]-Pro-[ζ-^{15}N]Lys-bR were prepared by growing *Halobacterium salinarum* in a defined medium similar to that of Gochnauer and Kushner (*26*), except that the D-amino acids and NH_4Cl were omitted. Isotopically enriched amino acids were substituted for natural abundance amino acids at a concentration of 0.085 g/L for Lys, 0.05 g/L for Pro, 0.05 g/L for Thr, 0.20 g/L for Tyr, and 0.33 g/L for Val. The specificity and efficiency of isotope incorporation was monitored using radiotracers. Extraction of samples with ammonia−acetone (1:5 by volume) indicated that ca. 38% of the radioactivity incorporated from lysine and ca. 14% of the radioactivity from valine went into lipids or retinal. However, amino acid analysis indicated that none of the radiotracers scrambled to other amino acid types.

PM patches were isolated from *H. salinarum* according to the conventional procedure (*27*). The purified sample was

suspended in a 0.3 M guanidine solution at pH 10.0 and allowed to stand for 30−120 min. Centrifugation of the PM suspension at a maximum of 43262*g* for 60 min produced a pellet, and the supernatant was removed. This process of washing and centrifugation was repeated until the supernatant remained at pH 10.0 (5−10 washes). The resulting pellet was packed into a transparent 5 mm quartz rotor.

Accumulation of LA. PM samples were light-adapted by illumination in situ for 1−2 h with the full visible spectrum of a 1000 W xenon lamp at 0 °C.

Accumulation of M_o. A sample in the LA state was cooled to −60 °C and illuminated in situ for 1−2 h with long-wavelength light from a xenon lamp using a 550 nm cutoff filter.

Accumulation of M_n. A sample in the LA state was cooled to −20 °C and illuminated in situ for 1−2 h with long-wavelength light from a xenon lamp using a 550 nm cutoff filter.

Solid-State NMR of Model Systems. ^{15}N and ^{13}C studies of model peptides were performed using custom-built spectrometers (courtesy of Dr. D. J. Rubin) operating at proton frequencies of 317 and 400 MHz, respectively. Because of the low natural abundance of ^{15}N and the long ^{1}H relaxation times in the model peptides studied, CP/MAS experiments were performed with a terminal 90° pulse on the ^{1}H channel to return the bulk magnetization to the magnetic field axis after acquisition. Typical recycle times ranged from 10 to 40 s. For ^{13}C, with its greater natural abundance and higher sensitivity, a reduced recycle time of 5 s was utilized to minimize data acquisition times. Spinning frequencies ranged from 1.5 to 3.0 kHz. The ^{15}N and ^{13}C chemical shifts were referenced to liquid ammonia and DSS, respectively, using standards of saturated (5.6 M) aqueous ammonium chloride (which is 26.9 ppm downfield from the signal of liquid ammonia) and TMS (which is 1.7 ppm downfield from the ^{13}C signal of DSS). As the ^{15}N chemical shift of proline is typically ca. 10 ppm downfield from other peptide signals, assignment was unambiguous for samples with only one labeled X−Pro pair. Unfortunately, assignment of ^{13}C chemical shifts was not as straightforward as for ^{15}N. Assignment was facilitated by reference to the large body of data for ^{13}C chemical shifts of peptides and proteins (*28*−*34*). The chemical shift tensor values are also helpful for determination of the carboxyl protonation state (*35*) and discrimination between carbonyl and carboxyl groups (unpublished results). Chemical shift tensors were determined from the spinning sideband manifold using the technique of Herzfeld and Berger (*36*). Spectral noise, as measured by the rms deviation of the signal-free regions, was used to determine error bars on individual sideband intensities.

Solid-State NMR of bR. All experiments on bR were performed at a ^{1}H frequency of 317 MHz. The custom-built triple resonance probe was equipped with a 5 mm Chemagnetics (Fort Collins, CO) spinning module and an optic fiber bundle for in situ sample illumination. Sample rotation rates were regulated within 5 Hz. To preserve photocycle intermediates, sample temperatures were maintained at a constant temperature below −70 °C and controlled within a 4 °C range, except as noted.

The rotational-echo double resonance (REDOR) pulse sequence shown in Figure 2 was utilized to recouple ^{13}C−^{15}N dipolar interactions in bR. By omitting the π pulses on the unobserved nuclei (^{13}C or ^{15}N), the heteronuclear couplings are not recoupled, and the reference or S_0 spectrum is obtained. Inclusion of the π pulses on the unobserved nuclei causes recoupling and produces a dephased or S spectrum. The difference between the two spectra, $S_0 - S$, yields only the signals which have dephased under ^{13}C−^{15}N couplings. A fixed REDOR mixing time of 2.667 ms (8 rotor periods) was utilized. Typical π pulse lengths were 5, 10, and 10 μs on the ^{1}H, ^{13}C, and ^{15}N channels, respectively. Cross-polarization contact times of 2 ms and recycle delays of 3 s were utilized.

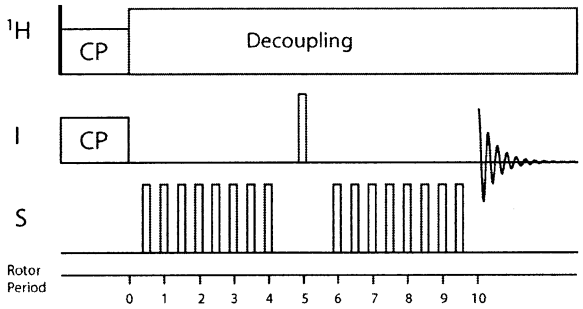

FIGURE 2: REDOR pulse sequence utilized for dipolar spectral editing.

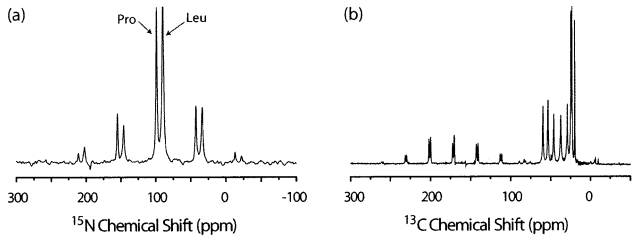

FIGURE 3: Typical (a) ^{15}N and (b) ^{13}C CP NMR spectra of the peptide cyclo-(Pro-Leu). The center band for each peptide nitrogen is identified.

^{13}C and ^{15}N chemical shifts were referenced to DSS and liquid ammonia, respectively, using TMS and 5.6 M ammonium chloride as external standards. The free lysine ζ-^{15}N resonance at 34.9 ppm and a ^{13}C resonance at 56.0 ppm were found to be invariant with temperature and utilized as internal chemical shift standards to ensure self-consistent referencing. Reported bR chemical shifts have a 0.5 ppm uncertainty.

RESULTS

X−Pro Model Peptides. Typical X−Pro peptide CP/MAS spectra are displayed in Figure 3, and Table 1 summarizes the chemical shift data for the model peptides, including several for which no crystal structure is available. Throughout, we will use the chemical shift convention $\delta_{11} \geq \delta_{22} \geq \delta_{33}$. The orientations of the principal axes of the peptide chemical shift tensors have been determined from measurements on single crystals (*37*, *38*) and powder samples (*39*−*41*). The upfield component, δ_{33}, is perpendicular to the peptide plane for both ^{13}C and ^{15}N. For ^{13}C, the δ_{11} and δ_{22} principal axes are approximately collinear with the C−Cα and C═O bonds, respectively. In the case of the ^{15}N tensor, the δ_{11} and δ_{22} elements lie in the peptide plane, with the latter aligned along the peptide bond. The span ($\Omega \equiv \delta_{11} - \delta_{33}$) of the X−Pro ^{15}N tensor (186 ± 15) is only slightly larger than that of other peptide bonds. However, the ^{15}N

Table 1: ^{13}C and ^{15}N Chemical Shift Data for X−Pro Model Peptides

	^{15}N (ppm)				^{13}C (ppm)				
compound	δ_{iso}	δ_{11}	δ_{22}	δ_{33}	δ_{iso}	δ_{11}	δ_{22}	δ_{33}	structure
Boc-**Pro**-Pro	98.9	186(3)	104(1)	9(2)	153.7	234	114	113	*cis* (*45*)
Z-**Pro**-Pro	102.4	146(2)	143(4)	18(2)	156.3	224	122	122	*cis* (*46*)
Leu-Pro-HCl	123.1	224(1)	117(1)	31(1)	169.2	250	167	91	
cyclo-(Pro-Pro)	124.2	207(2)	133(1)	34(1)	166.3	243	163	94	*cis* (*47*)
Poly-Pro-II	125.2	221(2)	121(2)	34(1)	170.5	243	173	95	*trans* (*48*)
cyclo-(Pro-Leu)	125.9	229(1)	118(1)	33(1)	171.9	253	180	83	*cis* (*49*)
Z-Pro-**Pro**	126.1	215(2)	131(1)	34(2)	170.0	240	176	95	*trans* (*50*)
Poly-Pro-I	127.8	220(2)	120(2)	45(1)	171.5	242	179	94	*cis* (*46*)
Boc-Gly-Pro	129.2	229(2)	130(1)	30(2)	166.3	243	167	90	*trans* (*51*)
Z-Gly-Pro	129.2	230(2)	123(1)	36(2)	168.6	243	167	95	*trans* (*52*)
cyclo-(Pro-Pro)	129.5	217(1)	139(1)	34(1)	167.2	245	165	92	*cis* (*53*)
Boc-Ala-Pro	129.9	233(2)	117(3)	42(2)	174.2	255	180	89	*trans* (*48*)
Z-Gly-Gly-Pro	129.9	232(3)	117(6)	42(6)	167.1	256	152	94	*trans* (*54*)
cyclo-(Gly-Pro)	130.9	231(3)	121(3)	42(3)	172.2	237	185	94	*cis* (*55*)
Ac-Pro-NHMe	131.4	227(2)	143(3)	26(2)	172.5	260	181	77	*trans* (*56*)
Z-Ala-Pro	131.4	239(2)	123(2)	34(2)	172.4	245	184	89	*trans* (*57*)
Ala-Pro	132.2	230(2)	114(4)	55(4)	169.3	248	172	88	
Gly-Pro	132.6	230(2)	114(4)	56(3)	165.7	239	166	92	
cyclo-(Met-Pro)	132.6				170.7	245	174	93	*cis* (*25*)
Ac-Pro-NH_2	132.8	240(4)	122(2)	38(2)	172.3	238	187	92	*trans* (*58*)
Boc-Pro-**Pro**	134.2	233(3)	146(1)	26(2)	174.1	237	193	92	*trans* (*45*)
Ac-Pro	134.4	236(1)	115(2)	54(2)	172.2	244	190	83	
Ala-Pro-Gly-H_2O	134.5	231(2)	124(2)	51(2)	169.2	240	175	93	*trans* (*59*)
Pr-Pro	135.7	239(1)	119(2)	51(2)	177.5	249	202	81	*cis* (*60*)
Gly-Pro	136.4	235(2)	132(2)	44(2)	167.2	245	166	90	
Val-Pro-HCl	139.4	254(3)	106(8)	60(8)	169.9	233	186	91	
Val-Pro-HCl	144.0	249(3)	119(5)	65(5)	172.8				
Phe-Pro-H_2O	145.1	237(4)	158(1)	43(3)	167.7	243	172	88	*cis* (*61*)

tensor of proline is much less axially symmetric than found in other amino acids, as indicated by a skew ($\kappa \equiv 3(\delta_{22} - \delta_{iso})/\Omega$) which is much closer to zero ($\kappa = -0.1 \pm 0.3$ compared to -0.7 ± 0.2) (*39*, *40*, *42*).

In the X−Pro peptide bonds, the δ_{11} and δ_{33} components of the ^{13}C tensor exhibit little variation. As the δ_{22} element is nearly collinear with the C═O bond, its variation may reflect changes in hydrogen bonding of the carbonyl oxygen. Hydrogen bonding reduces the double bond character of the C═O bond and increases the double bond character of the peptide bond. These changes alter the hybridization of the nitrogen in turn, which is observed to influence all three ^{15}N tensor elements.

Chemical shift data were analyzed for correlations to structural parameters such as bond lengths, hydrogen bonding, and dihedral angles using the multivariate linear regression package from the International Mathematics and Statistics Library (Visual Numerics, Inc.). In the analysis, the dependence of the chemical shift tensor principal values or any combination thereof upon the structural parameters was investigated. However, the only correlation found was between the ^{15}N isotropic chemical shift and the difference between the C−N and C═O bond lengths for *cis* peptides. As shown in Figure 4, the ^{15}N isotropic chemical shift moves downfield when the difference between the C−N and C═O bond lengths decreases. This decrease in relative bond lengths indicates increased mixing of bond orders of the C−N and C═O bonds and is expected to originate from hydrogen bonding to the carbonyl oxygen. However, this correlation is not observed for the *trans* peptides.

While few clear trends were observed, the broad range of isotropic ^{15}N chemical shifts and principal values indicate the sensitivity of the amide ^{15}N resonance to the local environment. On the other hand, the carbonyl ^{13}C chemical shift appears to be much less sensitive to local structure, with only the δ_{22} tensor element varying substantially between the model compounds. While the chemical shift differences between the β-^{13}C and γ-^{13}C positions are more clearly diagnostic of the X−Pro peptide bond conformation (*8*), ^{15}N serves as a sensitive probe of the local environment that has advantages over the ^{13}C side chain positions with respect to site-specific assignment when multiple proline residues are present in a sample.

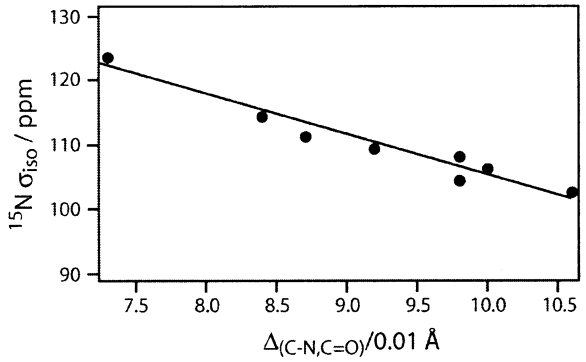

FIGURE 4: Correlation between the ^{15}N isotropic chemical shift and the difference between the C−N and C═O bond lengths for *cis* X−Pro peptides.

bR X−Pro Bonds. The ^{15}N spectrum of DA [1-^{13}C]Thr-[^{15}N]Pro-[ζ-^{15}N]Lys-bR (Figure 5) displays five distinct proline resonances distributed from 133.6 to 144.6 ppm, more than 10 ppm downfield from the other peptide ^{15}N signals (barely visible above the noise in Figure 5). Upon freezing, the signals broaden due to the suppression of line-narrowing motion. Nonetheless, the chemical shift distribution of the proline resonances remains at the low temperatures required to trap photocycle intermediates.

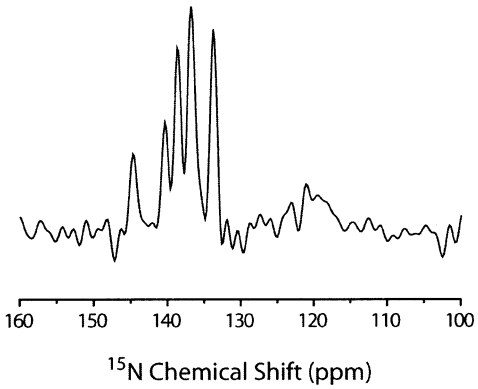

FIGURE 5: ^{15}N CP spectrum of DA [1-^{13}C]Thr-[^{15}N]Pro-bR at room temperature. Five distinct proline peaks are present between 132 and 145 ppm. These peaks are well resolved from the broad amide backbone line at ca. 120 ppm.

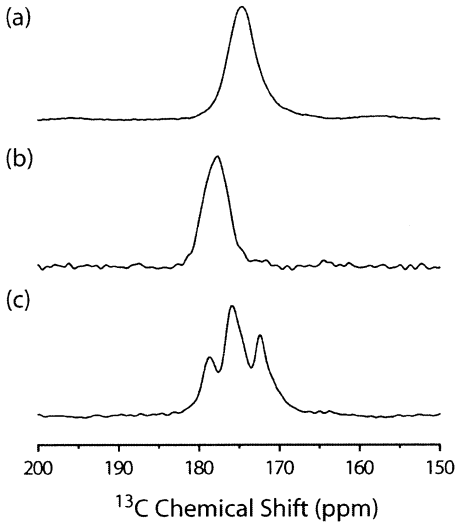

FIGURE 6: Comparison of the downfield region of the ^{13}C CP spectra of (a) [1-^{13}C]Thr-[^{15}N]Pro-[ζ-^{15}N]Lys-bR, (b) [1-^{13}C]Tyr-[^{15}N]Pro-[ζ-^{15}N]Lys-bR, and (c) [1-^{13}C]Val-[^{15}N]Pro-[ζ-^{15}N]Lys-bR.

The ^{13}C carbonyl spectra of the [1-^{13}C]Thr, [1-^{13}C]Tyr, and [1-^{13}C]Val labeled samples show fewer distinct peaks (Figure 6). However, the envelopes of carbonyl resonances in the three samples are quite distinct, suggesting that these residues populate diverse environments.

[1-^{13}C]Thr-[^{15}N]Pro-[ζ-^{15}N]Lys-bR. The use of REDOR filtering is demonstrated in Figure 7, where we isolate the ^{13}C signal from 1 of the 18 threonine residues present in the protein. Since Thr90-Pro91 represents the only Thr-Pro pair in bR, and therefore the only ^{13}C−^{15}N pair in the labeled sample, spectral assignment is straightforward. The ^{15}N and ^{13}C spin-pair filtered spectra of the LA, M_o, and M_n states of [1-^{13}C]Thr-[^{15}N]Pro-[ζ-^{15}N]Lys-bR are presented in Figure 8. The Pro91 ^{15}N chemical shift increases marginally (0.5 ppm) in the LA → M_o transition and remains constant between the two M states. The Thr90 ^{13}CO chemical shift remains constant at 174.0 ppm in all three states.

[1-^{13}C]Tyr-[^{15}N]Pro-[ζ-^{15}N]Lys-bR. As this sample contains only one directly bonded spin pair, Tyr185-Pro186, assignment of the filtered spectra in Figure 9 is again trivial. The Pro186 ^{15}N chemical shift increases slightly (0.6 ppm) upon M_o formation and remains constant in the later M_n state. The Tyr185 carbonyl ^{13}C chemical shift decreases from 177.6 ppm in the LA state to 175.9 ppm and 176.0 ppm in the early and late M states, respectively.

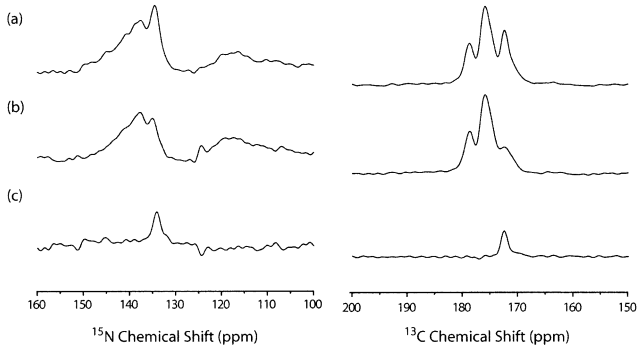

FIGURE 7: REDOR-filtered spectra of the backbone region of LA [1-^{13}C]Val-[^{15}N]Pro-[ζ-^{15}N]Lys-bR. For both nuclei, the downfield region is displayed for the (a) REDOR S_0 control, (b) REDOR S dephasing, and (c) REDOR S_0 − S difference spectra.

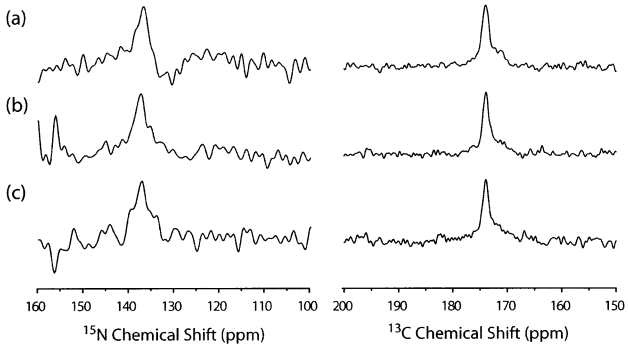

FIGURE 8: REDOR-filtered difference spectra of [1-^{13}C]Thr-[^{15}N]-Pro-[ζ-^{15}N]Lys-bR. For each nucleus, the downfield region is displayed for the (a) LA, (b) M_o, and (c) M_n states. The spurious signals at 154 and 160 ppm in the ^{15}N spectrum of (b) are due to an external rf source.

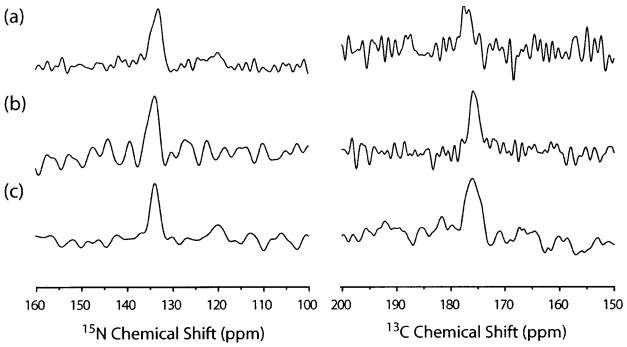

FIGURE 9: REDOR-filtered difference spectra of [1-^{13}C]Tyr-[^{15}N]-Pro-[ζ-^{15}N]Lys-bR. For each nucleus, the downfield region is displayed for the (a) LA, (b) M_o, and (c) M_n states.

[1-^{13}C]Val-[^{15}N]Pro-[ζ-^{15}N]Lys-bR. Three Val-Pro pairs exist in bR. The Val49-Pro50 pair is located in the B helix near the active site. In contrast, the Val69-Pro70 and Val199-Pro200 pairs are at the extracellular surface, in loops BC and FG, respectively. Consequently, three signals arise in the spin-pair filtered ^{15}N spectrum of DA [1-^{13}C]Val-[^{15}N]-Pro-[ζ-^{15}N]Lys-bR at room temperature (Figure 10a). These three signals have been provisionally labeled from upfield to downfield as Pro-A, Pro-B, and Pro-C. At room temperature, the resonance of Pro-A is sharper and more intense than the signals from Pro-B or Pro-C. Upon freezing of the sample to −70 °C, the signal due to Pro-A remains, while the signals from Pro-B and Pro-C become substantially

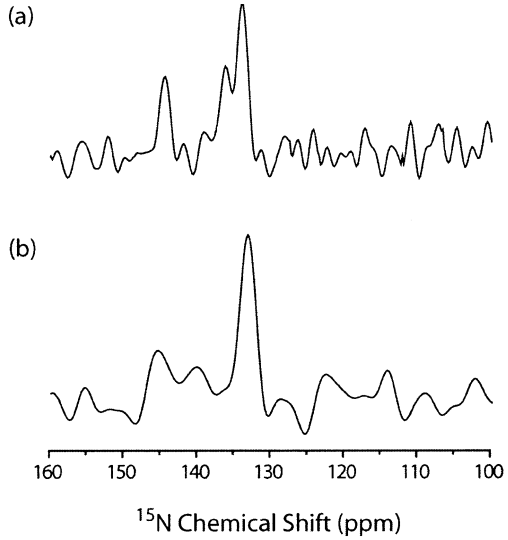

FIGURE 10: ^{15}N REDOR-filtered difference spectra of DA [1-^{13}C]-Val-[^{15}N]Pro-[ζ-^{15}N]Lys-bR at (a) room temperature and (b) −70 °C.

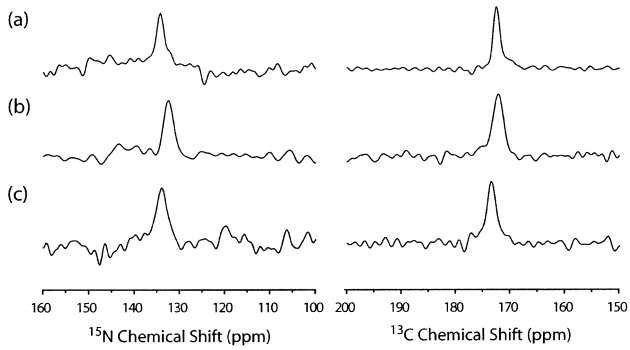

FIGURE 11: REDOR-filtered difference spectra of [1-^{13}C]Val-[^{15}N]-Pro-[ζ-^{15}N]Lys-bR. For each nucleus, the downfield region is displayed for the (a) LA, (b) M_o, and (c) M_n states.

weaker and all but vanish into the noise (Figure 10b). These results suggest that Pro-B and Pro-C are of similar species, while Pro-A is distinct. The lack of change upon freezing is consistent with Pro-A being located in a more rigid environment which cross-polarizes well even at room temperature and does not disorder greatly upon freezing. Conversely, Pro-B and Pro-C cross-polarize poorly at room temperature and become disordered upon freezing, which is consistent with residues in more flexible regions of the protein. Therefore, Pro-A is assigned to Pro50, which is part of a rigid helix, while Pro-B and Pro-C are assigned to the two Val-Pro pairs that are located in surface loops.

The rigid Val49-Pro50 pair can be clearly discerned in the thermally trapped photocycle intermediates (Figure 11) and is the focus of the subsequent discussion. The Pro50 ^{15}N chemical shift decreases slightly from 134.0 ppm in LA to 132.3 ppm in M_o and returns to 133.9 ppm in M_n. The Val49 carbonyl ^{13}C chemical shift decreases from 172.5 ppm in the LA state to 172.1 ppm in M_o and increases again to 173.4 ppm in M_n.

DISCUSSION

Val49 and Pro50. We find that the Pro50 ^{15}N chemical shift decreases by 1.7 ppm in the LA → M_o transition and returns to its original value in the M_o → M_n transition (Table 2). Such a pattern of perturbation and relaxation has been observed previously in other parts of the peptide backbone in bR (*43*) and in the hydrogen bonding of the indole nitrogen of at least one of the tryptophan residues (*44*). However, this timing does not match the opening of the cytoplasmic half-channel, which occurs a little later and persists much longer.

Table 2: ^{15}N Chemical Shifts (ppm) of the Buried Proline Residues in Various Photocycle Intermediates

	Pro50	Pro91	Pro186
LA	134.0	136.9	133.0
M_o	132.3	137.4	133.6
M_n	133.9	137.3	133.8

Table 3: 1-^{13}C Chemical Shifts (ppm) of the Neighbors of Buried Prolines in Various Photocycle Intermediates

	Val49	Thr90	Tyr185
LA	172.5	174.0	177.6
M_o	172.1	173.9	175.9
M_n	173.4	173.9	176.0

The Val49 ^{13}CO chemical shift does not change significantly upon M_o formation and increases only marginally in the transition to M_n. The Val49 ^{13}CO chemical shift in M_n is 0.9 ppm larger than in the LA state. These changes are very small compared to those that have been observed in the ^{13}CO chemical shifts of other valine residues (*43*). Thus, barring an unusual cancellation of effects, it seems that the Val49−Pro50 peptide bond is relatively unperturbed in the middle of the photocycle.

Thr90 and Pro91. The small chemical shift changes for Thr90 and Pro91 are within experimental error and suggest that the Thr90−Pro91 bond does not change significantly during the photocycle. While it is conceivable that by unfortunate coincidence a number of effects on the chemical shifts have acted in opposition to produce no net change despite a conformational change, the most straightforward interpretation is that the Thr90−Pro91 bond is unperturbed through the middle of the photocycle.

Tyr185 and Pro186. The location of Pro186 directly on the retinal binding pocket suggests that it may be involved in structural changes during the photocycle, and mutagenesis experiments indicate that replacement of Pro186 alters the visible spectrum and reduces the proton pumping (*10*). However, the spectra in Figure 8 indicate no significant change in the Pro186 ^{15}N chemical shift through the middle of the photocycle.

Tyr185 has been previously implicated in changes during the photocycle. FTIR spectroscopy indicates a shifted carbonyl stretch frequency of Tyr185 in the N photocycle intermediate (*14*). The NMR data also clearly indicate perturbation of the Tyr185 carbonyl during the photocycle. However, the chemical shift measurements indicate that this change has already occurred by the time of the early M state and remains unchanged in the late M state.

CONCLUSIONS

Investigation of 1-^{13}C and ^{15}N chemical shifts in X−Pro peptide bonds of numerous model compounds has revealed that the ^{15}N chemical shift is extremely sensitive to the local structure. While a clear correlation between the ^{15}N chemical

shift and the peptide bond conformation could not be established, changes in the peptide bond conformation do result in perturbation of the chemical shift. In contrast, the ^{13}C carbonyl chemical shift is less sensitive to local structure, and what little variation there is appears almost entirely in the δ_{22} tensor element.

Using REDOR to select spin pairs, the ^{15}N and ^{13}C chemical shifts of the three buried X−Pro peptide bonds of bR were determined in the LA, M_o, and M_n states. Three different patterns are observed. The Pro50 ^{15}N exhibits a small perturbation in the early M state which relaxes by the late M state. The Pro91 ^{15}N chemical shift is essentially unperturbed in both M states. The Pro186 ^{15}N chemical shift is perturbed slightly upon M formation and remains so in the later M state. In the last two cases, the behavior of the ^{15}N chemical shifts of the prolines is paralleled by the behavior of the ^{13}CO chemical shifts of their partners. The ^{13}CO chemical shift of Thr90 remains constant through all three states, and a small change in the ^{13}CO chemical shift of Tyr185 in early M persists in late M. However, the ^{13}CO chemical shift of Val49 is not coordinated with the ^{15}N chemical shift of Pro50. The Val49 carbonyl is unperturbed in early M but becomes slightly perturbed in late M.

What relationship might these changes have to do with the accessibility switch of the pump or the helix movements seen in cyroelectron microscopy? In order to function as an accessibility switch, protein conformational change must occur while the Schiff base is deprotonated (i.e., during the lifetime of the M state). This is also the period during which helices are perturbed from their resting state conformation in native membranes. The only X−Pro chemical shift changes that we see between the early and late M states are in the Val49−Pro50 peptide bond. However, the ^{15}N shifts of Pro50 suggest that the formation of M_n relaxes an earlier perturbation back to the resting state, and therefore this change is not likely to serve as the accessibility switch or be associated with the observed movement of the B helix. Meanwhile, the early timing and small magnitudes of the changes in the Tyr185-Pro186 chemical shifts suggest that the hinge point for the tilting of the cytoplasmic portion of the F helix is probably located elsewhere in the protein. Overall, the absence of evidence for structural change in the vicinity of the buried X−Pro bonds specifically during the critical transition from the early M state (in which the chromophore has just deprotonated to the extracellular half-channel) to the late M state (in which the chromophore is about to be reprotonated from the intracellular half-channel) suggests that the buried proline residues play a purely structural role in bR.

ACKNOWLEDGMENT

The authors thank Dr. Nathan Astrof for helpful discussions.

REFERENCES

1. Yun, R. H., Anderson, A., and Hermans, J. (1991) *Proteins: Struct., Funct., Genet. 10*, 219−228.
2. Riek, R. P., Rigoutsos, I., Novotny, J., and Graham, R. M. (2001) *J. Mol. Biol. 306*, 349−362.
3. del Camino, D., Holmgren, M., Liu, Y., and Yellen, G. (2000) *Nature 403*, 321−325.
4. Tieleman, D. P., Shrivastava, I. H., Ulmschneider, M. R., and Sansom, M. S. P. (2001) *Proteins: Struct., Funct., Genet. 44*, 63−72.
5. Deber, C. M., Sorrell, B. J., and Xu, G.-Y. (1990) *Biochem. Biophys. Res. Commun. 172*, 862−869.
6. Gerwert, K., Hess, B., and Englehard, M. (1990) *FEBS Lett. 261*, 449−454.
7. Williams, K. A., and Deber, C. M. (1991) *Biochemistry 30*, 8919−8923.
8. Englehard, M., Finkler, S., Metz, G., and Siebert, F. (1996) *Eur. J. Biochem. 235*, 526−533.
9. Lu, H., Marti, T., and Booth, P. J. (2001) *J. Mol. Biol. 308*, 437−446.
10. Mogi, T., Stern, L. J., Chao, B. H., and Khorana, H. G. (1989) *J. Biol. Chem. 264*, 14192−14196.
11. Rothschild, K. J., He, Y.-W., Mogi, T., Marti, T., Stern, L. J., and Khorana, H. G. (1990) *Biochemistry 29*, 5954−5960.
12. Zhang, Y. N., El-Sayed, M. A., Stern, L. J., Marti, T., Mogi, T., and Khorana, H. G. (1993) *Photochem. Photobiol. 57*, 1027−1031.
13. Rothschild, K. J., He, Y.-W., Gray, D., Roepe, P. D., Pelletier, S. L., Brown, R. S., and Herzfeld, J. (1989) *Proc. Natl. Acad. Sci. U.S.A. 86*, 9832−9835.
14. Ludlam, C. F. C., Sonar, S., Lee, C.-P., Coleman, M., Herzfeld, J., RajBhandary, U. L., and Rothschild, K. J. (1995) *Biochemistry 34*, 2−6.
15. Vonck, J. (1996) *Biochemistry 35*, 5870−5878.
16. Subramaniam, S., Lindahl, M., Bullough, P., Faruqi, A. R., Tittor, J., Oesterhelt, D., Brown, L., Lanyi, J., and Henderson, R. (1999) *J. Mol. Biol. 287*, 145−161.
17. Luecke, H., Schobert, B., Richter, H.-T., Cartailler, J.-P., and Lanyi, J. K. (1999) *Science 286*, 255−260.
18. Sass, H. J., Buldt, G., Gessenich, R., Hehn, D., Neff, D., Schlesinger, R., Berendzen, J., and Ormos, P. (2000) *Nature 406*, 649−653.
19. Gamble, T. R., Vajdos, F. F., Yoo, S., Worthylake, D. K., Houseweart, M., Sundquist, W. I., and Hill, C. P. (1996) *Cell 87*, 1285−1294.
20. Bosco, D. A., Eisenmesser, E. Z., Pochapsky, S., Sundquist, W. I., and Kern, D. (2002) *Proc. Natl. Acad. Sci. U.S.A. 99*, 5247−5252.
21. Luecke, H., Schobert, B., Richter, H.-T., Cartailler, J.-P., and Lanyi, J. K. (1999) *J. Mol. Biol. 291*, 899−911.
22. Essen, L.-O., Siegert, R., Lehmann, W. D., and Oesterhelt, D. (1998) *Proc. Natl. Acad. Sci. U.S.A. 95*, 11673−11678.
23. Belrhali, H., Nollert, P., Royant, A., Menzel, C., Rosenbusch, J. P., Landau, E. M., and Pebay-Peyroula, E. (1999) *Structure 7*, 909−917.
24. Greenstein, J. P., and Winitz, M. (1961) *Chemistry of the Amino Acids*, Vol. 2, Wiley, New York.
25. Padmanabhan, V. M., and Jakkal, V. S. (1987) *Acta Crystallogr., Sect. C 43*, 349−351.
26. Gochnauer, M. B., and Kushner, D. (1969) *Can. J. Microbiol. 15*, 1157−1165.
27. Oesterhelt, D., and Stoeckenius, W. (1973) *Methods Enzymol. 31*, 667−678.
28. Ando, S., Matsumoto, K., and Ando, I. (1989) *J. Mol. Struct. 212*, 123−135.
29. Asakawa, N., Kuroki, S., Kurosu, H., Ando, I., Shoji, A., and Ozaki, T. (1992) *J. Am. Chem. Soc. 114*, 3261−3265.
30. Flippen-Anderson, J. L., Gilardi, R., Karle, I. L., Frey, M. H., Opella, S. J., Gierasch, L. M., Goodman, M., Madison, V., and Delaney, N. G. (1983) *J. Am. Chem. Soc. 105*, 6609−6614.
31. Garbay-Jaureguiberry, C., Arnoux, B., Prange, T., Altenburger, S., Pascard, C., and Roques, B. P. (1980) *J. Am. Chem. Soc. 102*, 1827−1837.
32. Kricheldorf, H. R., Haupt, T. K., and Muller, D. (1986) *Magn. Reson. Chem. 24*, 41−52.
33. Muller, D., Stulz, J., and Kricheldorf, H. (1984) *Makromol. Chem., Macromol. Chem. Phys. 185*, 1739−1749.
34. Sarkar, S. K., Torchia, D. A., Kopple, K. D., and van der Hart, D. L. (1984) *J. Am. Chem. Soc. 106*, 3328−3331.
35. Gu, Z. T., and McDermott, A. (1993) *J. Am. Chem. Soc. 115*, 4282−4285.
36. Herzfeld, J., and Berger, A. E. (1980) *J. Chem. Phys. 73*, 6021−6030.
37. Harbison, G. S., Jelinski, L. W., Stark, R. E., Torchia, D. A., Herzfeld, J., and Griffin, R. G. (1984) *J. Magn. Reson. 60*, 79−82.

38. Stark, R. E., Jelinski, L. W., Ruben, D. J., Torchia, D. A., and Griffin, R. G. (1983) *J. Magn. Reson. 55*, 266−273.
39. Hartzell, C. J., Whitfield, M., Oas, T. G., and Drobny, G. P. (1987) *J. Am. Chem. Soc. 109*, 5966−5969.
40. Oas, T. G., Hartzell, C. J., Dahlquist, F. W., and Drobny, G. P. (1987) *J. Am. Chem. Soc. 109*, 5962−5966.
41. Oas, T. G., Hartzell, C. J., McMahon, T. J., Drobny, G. P., and Dahlquist, F. W. (1987) *J. Am. Chem. Soc. 109*, 5956−5962.
42. Shoji, A., Ozaki, T., Fujito, T., Deguchi, K., Ando, I., and Magoshi, J. (1998) *J. Mol. Struct. 441*, 251−266.
43. Hu, J. G., Sun, B. Q., Bizounok, M., Hatcher, M. E., Lansing, J. C., Raap, J., Verdegem, P. J. E., Lugtenburg, J., Griffin, R. G., and Herzfeld, J. (1998) *Biochemistry 37*, 8088−8096.
44. Petkova, A. T., Hatanaka, M., Jaroniec, C. P., Hu, J. G., Belenky, M., Verhoeven, M., Lugtenburg, J., Griffin, R. G., and Herzfeld, J. (2002) *Biochemistry 41*, 2429−2437.
45. Kamwaya, M. E., Oster, O., and Bradaczek, H. (1981) *Acta Crystallogr., Sect. B 37*, 1564−1568.
46. Blessing, R. H., and Smith, G. D. (1982) *Acta Crystallogr., Sect. B 38*, 1203−1207.
47. Benedetti, E., Goodman, M., Marsh, R. E., Rapoport, H., and Musich, J. A. (1975) *Cryst. Struct. Commun. 4*, 641.
48. Arnott, S., and Dover, S. D. (1968) *Acta Crystallogr., Sect. B 24*, 599.
49. Karle, I. L. (1972) *J. Am. Chem. Soc. 94*, 81.
50. Traub, W., and Shmueli, U. (1963) *Nature 4886*, 1165.
51. Benedetti, E., Palumbo, M., Bonora, G. M., and Toniolo, C. (1976) *Macromolecules 9*, 417.
52. Tanaka, I., Kozima, T., Ashida, T., Tanaka, N., and Kakudo, M. (1977) *Acta Crystallogr., Sect. B 33*, 116−119.
53. Kamwaya, M. E., Oster, O., Bradaczek, H., Ponnuswamy, M. N., Parthasarathy, S., Nagaraj, R., and Balaram, P. (1982) *Acta Crystallogr., Sect. B 38*, 172−176.
54. Wu, S., Tinant, B., DeClercq, J. P., and Van Meerssche, M. (1987) *Bull. Soc. Chim. Belg. 96*, 437−441.
55. Von Dreele, R. B. (1975) *Acta Crystallogr., Sect. B 31*, 966−970.
56. Matsuzaki, T., and Iitaya, Y. (1971) *Acta Crystallogr., Sect. B 27*, 507.
57. Panneerselvam, K., Chacko, K. K., and Veena, K. R. (1990) *Acta Crystallogr., Sect. C 46*, 81−84.
58. Druck, U., Littke, W., and Main, P. (1979) *Acta Crystallogr., Sect. B 35*, 253−255.
59. Wu, S., DeClercq, J. P., Tinant, B., and Van Meerssche, M. (1987) *Bull. Soc. Chim. Belg. 96*, 515−520.
60. Kamwaya, M. E., Oster, O., and Bradaczek, H. (1981) *Acta Crystallogr., Sect. B 37*, 364−367.
61. Panneerselvam, K., and Chacko, K. K. (1989) *Acta Crystallogr., Sect. C 45*, 106−109.

BI027042F